CAVITATING INDUCER INSTABILITIES: EXPERIMENTAL ANALYSIS AND 2D NUMERICAL SIMULATION OF UNSTEADY FLOW IN BLADE CASCADE.

F. Joussellin, Y. Courtot, O. Coutier-Delgosha, J.L. Reboud [(*)]
Laboratoire des Ecoulements Géophysiques et Industriels, Grenoble, France
[(*)] ENISE/LTDS, Saint Etienne, France

Abstract
Cavitating flows in rocket engine turbo-pump inducers are studied by experimental and numerical ways. The experimental analysis focused on the cavitating structures at the periphery of the inducer, the quantification of the vapour volume at inducer inlet, its relation with the backflow and the obstruction effect on the main flow. A 2D numerical model of unsteady cavitation was applied to a blade cascade drawn from the inducer geometry. Unsteady behaviour of sheet cavities attached to the blade suction side depends on the flow rate and cavitation number. In certain conditions, a rotating cavitation phenomenon is observed, in good agreement with experimental observations.

Nomenclature

$\boldsymbol{C}$ *(Cm, Cu)*	Velocity vector in fixed frame	$Cm=Q/Sflow$
p, P	Static pressure, total pressure	$P = p + 0.5\ r_l\ \boldsymbol{C}^2$
U	Training velocity at inducer tip radius R	$U = R\ W$
s	Cavitation parameter	$(P_1-p_v) / (0.5\ r_l\ R^2W^2)$
F	Flow coefficient	$Q / (RW)$
Y	Head coefficient	$(P_2-P_1)/(\ r_l\ R^2W^2)$
r_l, r_v, r	Density of the liquid, of the vapour, of the mixture	

1. Introduction
To achieve operating at high rotational speed and low inlet pressure, rocket engines turbo pumps are generally equipped with an axial inducer stage. Under such operating conditions, cavitation develops on suction side of the blades and at inducer periphery near the tip. Peripheral cavitation concerns all cavitating structures that appear near the shroud casing at the inducer inlet, as backflow of the pump (Yokata *et al.*, 1999) and cavitating tip vortices (Laborde *et al.*, 1995).
When inlet pressure is decreased from cavitation inception to breakdown of the pump, unsteady phenomena may appears, associated with different blade cavitation patterns. In Figure 1, successive flow patterns are located on the performance curve of a liquid hydrogen inducer (de Bernardi *et al.*, 1993).
At cavitation inception, a steady and balanced flow pattern with one short attached cavity on each blade is observed from flow visualisations. When cavitation parameter is slightly decreased, a steady and alternate cavitating configuration appears (only on four blades inducers) with alternatively one short and one long cavity. Then flow visualisations achieve to identify an unsteady flow pattern. Rotating cavitation appears at low cavitation parameter (Kamijo *et al.*, 1977) just above breakdown. Unbalanced attached cavities are observed in the different channels, their distribution rotating faster than the inducer (de Bernardi *et al.*, 1993; Pagnier *et al*, 1995) and leading to large radials loads on the shaft (Goirand *et al.*; 1992). Finally near the breakdown of the inducer, a steady and balanced flow pattern with fully developed cavitation is observed.
Over the last few years, numerical models have been developed to predict the cavitation instability in inducers. These models are based on stability analyses and linear approach, taking into account the total flow rate variations through a cavitating blade-to-blade channel (Tsujimoto *et al.*, 1993; Joussellin & de Bernardi, 1994), or calculating the flow around attached cavities (Pilipenko *et al.*, 1995; Watanabe *et al.*, 1998).
To improve the understanding and the prediction capability of cavitation instabilities, numerical and experimental analyses are developed through collaborations between the LEGI, the Rocket Engine Division of SNECMA Moteurs and the French space agency CNES. In this paper, experimental analysis focuses on the size of peripheral cavitating

structures and their influences on the inlet flow. In parallel, the cavitation behaviour of inducers is simulated using a 2D model of unsteady cavitating flow developed at LEGI (Reboud & Delannoy, 1994; Coutier-Delgosha *et al.*, 2000).

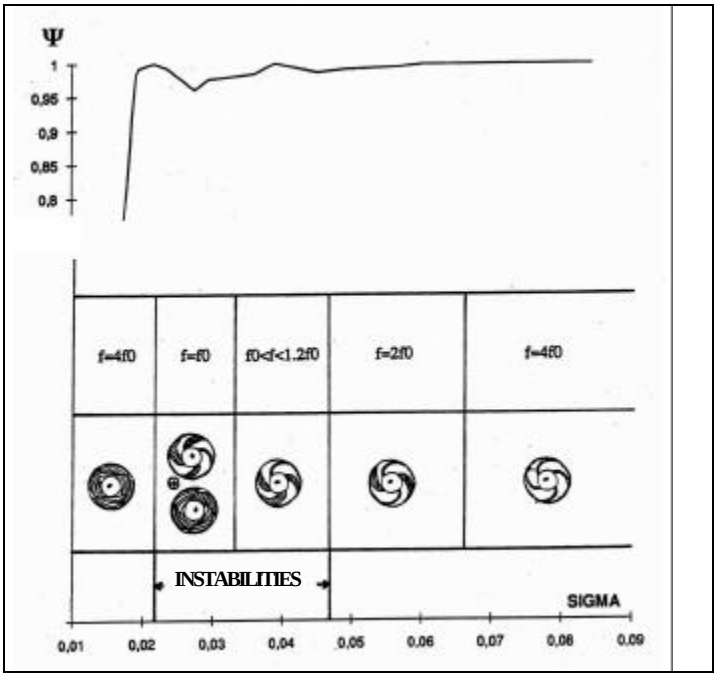

Figure 1. Sketches of cavitation patterns for various cavitation parameters and their correspondence to the performance curve (de Bernardi *et al.*,1993).

2. Cavitation in inducer: description of different types of cavitation

There are many types of cavitation in inducers. The cavitation depends on inducer geometry (leading edge) and on operating conditions. Cavitation in such inducer could appear in 2 regions well separated (Figure 2.): on the blade (b), or at peripheral zone (p).

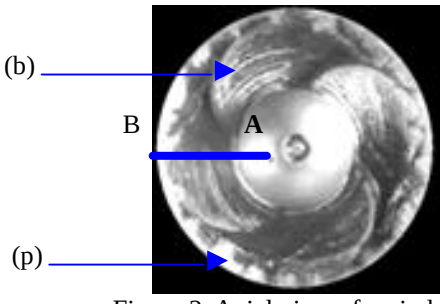

Figure 2. Axial view of an inducer

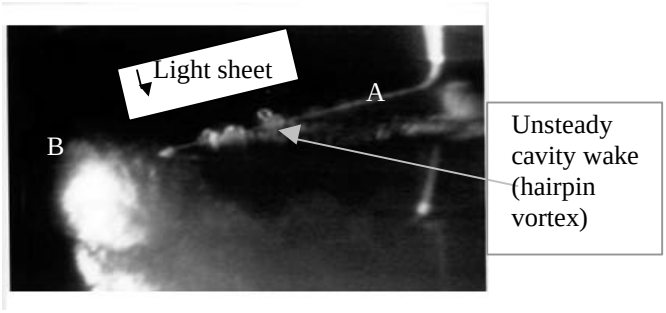

Figure 3. Radial view obtained with light sheet illumination of an inducer radius (AB).

The case of swept back leading edge leads to small pressure gradient in radial direction. Then cavitation could appear on the entire blade, from hub to tip radius. In that case, the cavitation sheet volume is maximum at about 5% of the blade to blade volume, which is very small compare to peripheral zone where it could be really large at low flow rate (Joussellin *et al.*, 1998). The behaviour of cavitation on this blade is similar to the one appearing in 2D facility with hairpins vortices in the unsteady cavity wake (see Figure 3 a radial view obtaining with a light sheet perpendicular to the blade, following AB). In the case of a more radial leading edge design, the pressure gradient versus radius is high, and low pressure zone i.e. cavitation is limited to the periphery of inducer.

At peripheral zone, cavitation is mainly related to the tip leakage flow:

The pressure difference between the 2 sides of a blade causes a tip leakage flow to pass through the tip clearance which leads to a reverse flow (against active flow) which generates 3 types of cavitation (Figure 4):

- ***Tc- tip clearance cavitation*:** it is defined as the cavitation *in* the tip clearance (between the tip surface of the blade and the casing); it is in fact a form of blade cavitation on the tip surface and it depends on the geometry of the tip (Laborde *et al.*, 1995).
- ***Tv - tip vortex cavitation:*** the tip leakage flow induces a shear layer that rolls up to form the tip vortex, which is similar to such of a wing. The cavitation in an inducer first appears in the tip vortex (at cavitation inception)
- ***$T_{s\ell}$ - tip shear layer cavitation:*** Between blade and tip vortex, there is a shear layer formed by the tip leakage flow which is turbulent, and could cavitate.

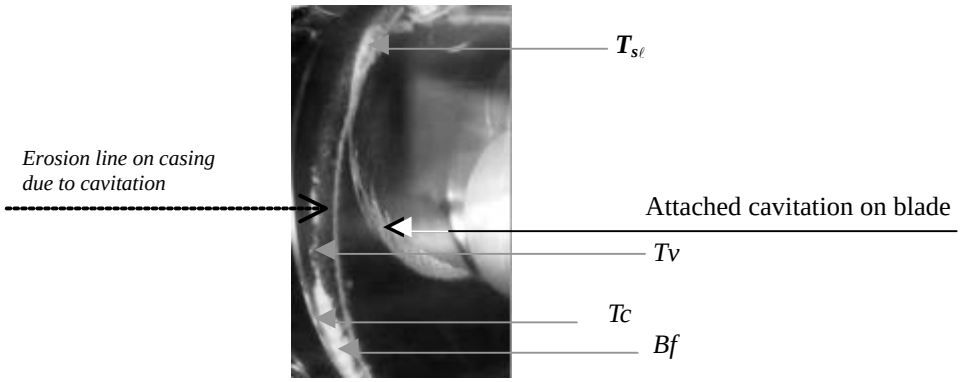

Figure 4**.** Scheme of cavitation in inducer: *Bf*- backflow vortex cavitation, *Tv* - tip vortex cavitation, $T_{s\ell}$ - tip shear layer cavitation, *Tc*- tip clearance cavitation, in inducer tip.

On the other hand, as a shear layer is formed between the swirling reverse flow and the non-rotational inlet flow, backflow vortices are formed and generates cavitation, called "backflow vortex cavitation" (Figure 4.), due to the fact that inducers are used at low flow rate, with incidence non equal to zero:

- ***Bf - backflow vortex cavitation*:** it generates an adverse flow; this type of cavitation could be the major mode of cavitation which could grow and take all peripheral place.

Interaction exists between these different types of cavitation; the main volume occupied by cavitation could be attributed to backflow phenomenon.

3. Experimental facility and image processing results

As we want to quantify all type of peripheral cavitation, we use only axial view as it is shown above:
The size of peripheral cavitation is obtained by image processing of the front view of the inducer (Figure 5a.), using the fact that cavitation appears clearly on these pictures (Figure 5b.).

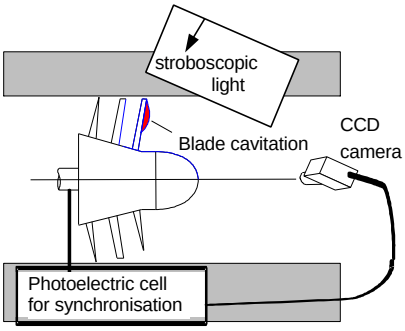

Figure 5a. Experimental facility

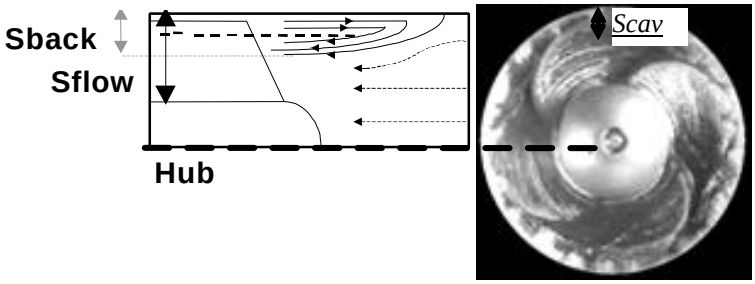

Figure 5b. Inlet inducer flow with backflow area.

From standard video acquisition images, cavitating region is extracted using National Institute of Health image processing code; the 4 main steps (Figure 6.) are (a) selection of the inducer without casing, and (b) filtering the entire picture by withdrawn the average intensity obtained on a 16x16 pixels zone. Then, (c) white pixels corresponding to the cavitating region are extracted (by selecting only the white region adjacent to the inducer diameter); then, the corresponding pixels are counted to get the area containing the cavitation structures, S_{cav}.

Some remarks on this method:
First point, it has been used in the case of standard video, although the frequency of the phenomenon of instability is higher. The next step is to use high-speed video. Second point, axial image are used, taking about 1 meter in front of

the inducer, then such axial image take into account all the upstream cavitation which appears between blade and video camera: this upstream expansion could be quantify on another new image, as Figure 3 or 4.

a) Original image, without casing	b) Using fonction Substrack background	c) Peripheral cavitation extraction	d) Comparison between original image (with casing) and extraction (c)
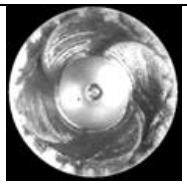			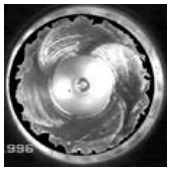

Figure 6. The 4 steps of image processing to obtain peripheral cavitation (in black, (c&d)).

For a given flow rate (Figure 7.), cavitating region, Scav, appears constant at ± 10% with respect to the cavitation parameter. On the other hand, for a given cavitation parameter (Figure 8.), Scav (image processing results, points ⋇), decreases linearly when the flow rate, Q/Qo, increases (where Qo is the design flow rate with a zero incidence at inducer tip). These results agree with those presented by Yokata *et al*. (1999).

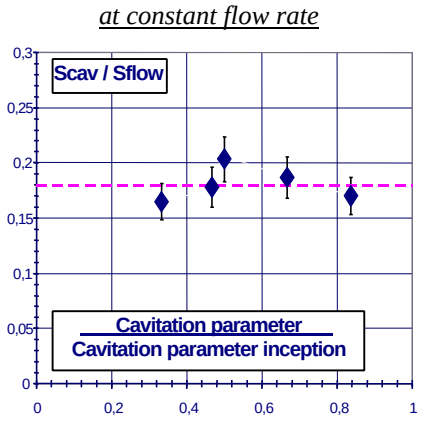

Figure 7**.** Evolution of flow sections, Scav, versus cavitation parameter.

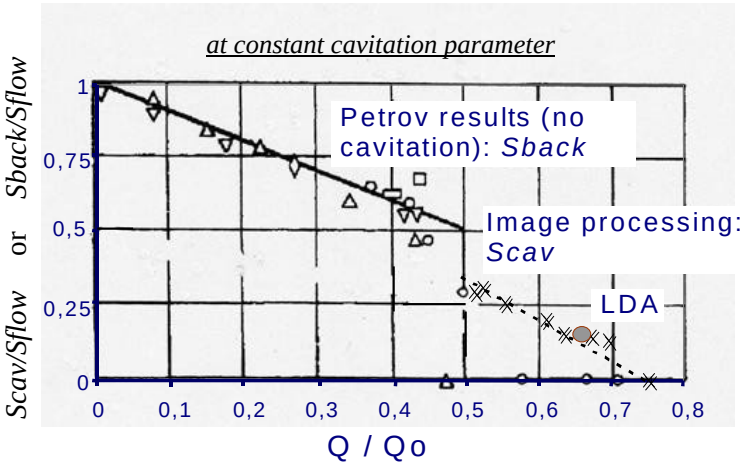

Figure 8**.** Evolution of flow sections, Scav and Sback, versus flow rate (Q/Q_0),

This behaviour is similar to the evolution of the backflow section (Sback mentioned in Figure 5b.) with the flow rate (Figure 8.), which has been highlighted in Russian inducers studies (Petrov & Chebayevsky, 1973). This result leads to conclude that cavitation appears in backflow zone without strongly modifying its expansion. LDA measurements performed in CREMHyG laboratory (Von Kaenel *et al.*, 1995), cf. point • in Figure 8, confirm that peripheral cavitation area, Scav, deduced from visualization coincides with backflow area in non-cavitating conditions.
In conclusion, the obstruction of the flow section by the cavitating backflow area modifies the inlet axial velocity Cm with respect to the uniform value Q/Sflow. That phenomenon must be kept in mind to analyse the results of 2D numerical simulations.

4. Unsteady cavitating flow model in 2D blade cascade

Numerical simulation of the cavitating flow in the inducer was performed with the objective to take into account the cavitation sheets attached to the blades and their unsteady behaviour. The 2D numerical model of unsteady cavitating flow, developed in previous studies (Delannoy & Kueny, 1990, Reboud & Delannoy, 1994, Reboud *et al.* 1998), was adapted to 2D blade cascades (Coutier-Delgosha *et al.* 2000). The main features of the models are:

- The liquid-vapour mixture is described as a single fluid, whose density r rapidly varies between the pure liquid density r_l and the pure vapour one r_v when the static pressure in the flow field reaches the vapour pressure. The fluid density is managed by a barotropic state law $r(p)$, as in (Coutier-Delgosha *et al.*, 2001).

- 2D unsteady Reynolds averaged Navier-Stokes equations are applied to that single fluid with variable density. The turbulence model used is the classical k-ε model, associated with laws of the wall along solid boundaries.
- Other boundary conditions are: imposed velocity at the mesh inlet (the flow velocity is deduced from the classical value Q/Sflow), imposed static pressure at the outlet, and periodicity or connection conditions between the different channel of the blade cascade. These conditions are applied along non-matching boundaries, through a special treatment developed in (Coutier-Delgosha *et al*., 2000) to assure the best transfer of both mass and momentum fluxes.

Computations are performed in a four blades cascade representing a complete inducer. The 2D blade-to-blade channels were drawn by cutting the 3D inducer geometry at constant radius equal to 70% of the tip radius R (Figure 9.). Taking into account the real radius and thickness evolutions of the stream-sheet crossing the inducer would be possible by using a S1/S2 approach, but the numerical model has not yet been adapted to that formulation. We use a 190x30 structured mesh per channel, giving a total of 22800 internal nodes when calculating the 4 blades cascade.

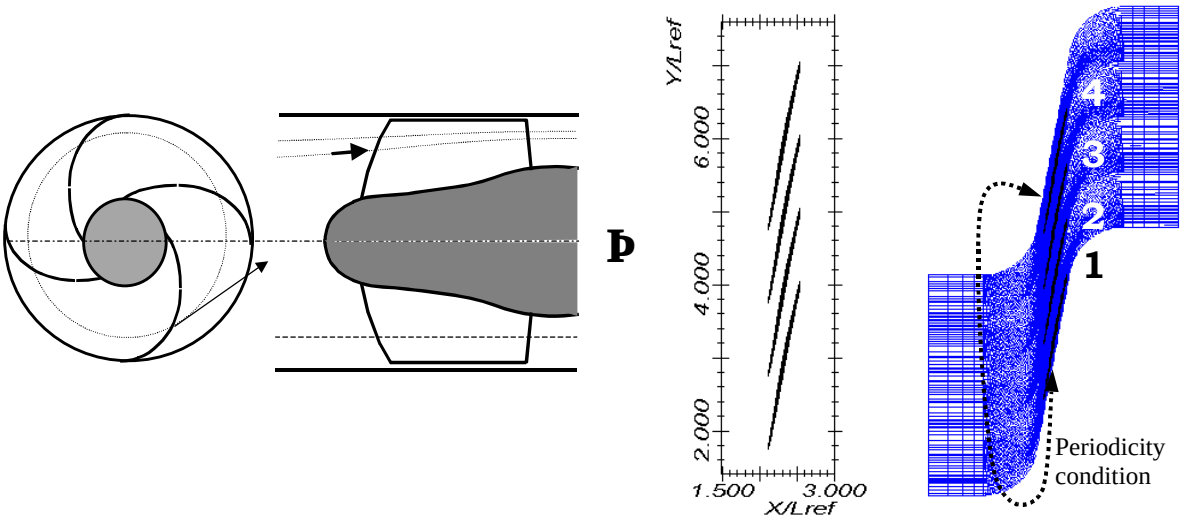

Figure 9. Description of the blade cascade obtained from the inducer geometry, and the 22800 nodes mesh.

5. Single-channel computation

In that first case, only one channel is computed, associated with a periodicity condition. A slow decrease of the cavitation number, from the non-cavitating condition provides at given flow coefficient the cascade cavitation performance. Large time steps are imposed during that slow transient, to minimise the time dependant terms of the discretized equation and to obtain quasi-steady flow fields. Some numerical instability is observed when the cavitating flow is fundamentally unstable. That is more particularly the case when reaching the final head drop: the flow rate is imposed strictly at the inlet and the cavitation blockage is thus especially abrupt. When σ values decrease, cavitation performance curve shows (Figure 10.) a first drop and the increase of the head just before the final blockage. Observation of the velocity fields shows that the phenomenon is due the interaction between the attached sheet cavitation and the boundary layer in the blade-to-blade channels.

6. Multiple-channels computations

Unsteady computations are performed on the 4 blades mesh. The periodicity condition is then applied between the 4^{th} and 1^{st} channels, as is the real runner. The time step, mesh and turbulence model are chosen to put the attention on the low frequency fluctuations of the attached cavity, more than to the local unsteadiness in the cavitation sheet wake (cloud shedding): the time step if fixed equal to 1% of the blade passage time t_{ref}.

Successive time accurate computations are performed at fixed cavitation number and flow rate coefficient. First cases with quite high cavitation number ($\sigma \approx 0.1$) lead to stable and symmetrical small cavities attached on each blade (Figure 11a.), their shape is then exactly the same than in the single-channel computation.

Figure 11b shows the flow rates passing the different channels, there are constant at a value around 25% of the total flow rate (the initial flow rate transient correspond to the growing of the 4 attached cavities from the non cavitating initial condition).

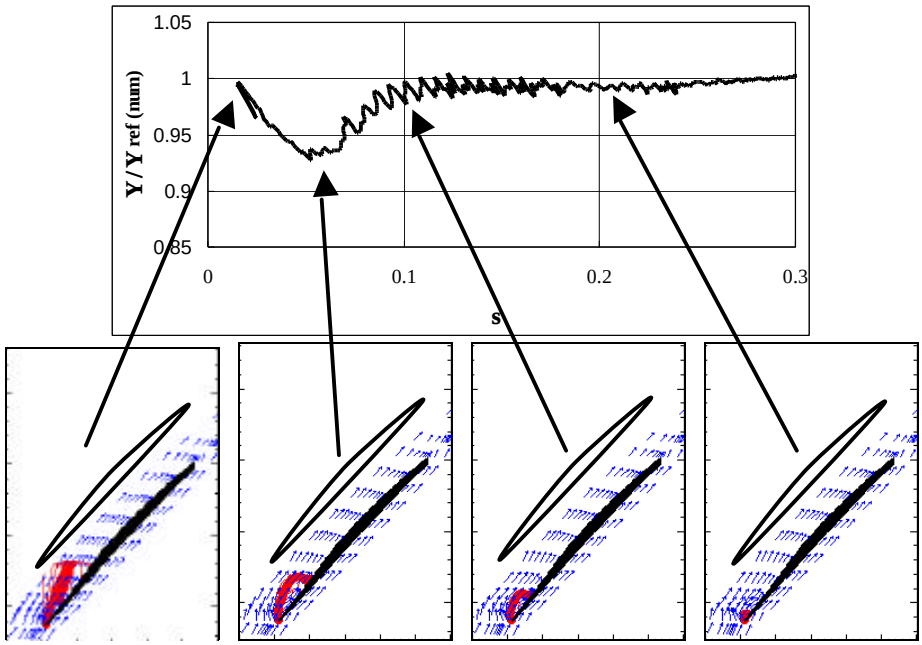

Figure 10. Single channel computation: cavitation characteristic of the cascade at $\phi = \phi_{ref}$, associated extension of the attached cavity (ratio 5:1 between horizontal and vertical scales).

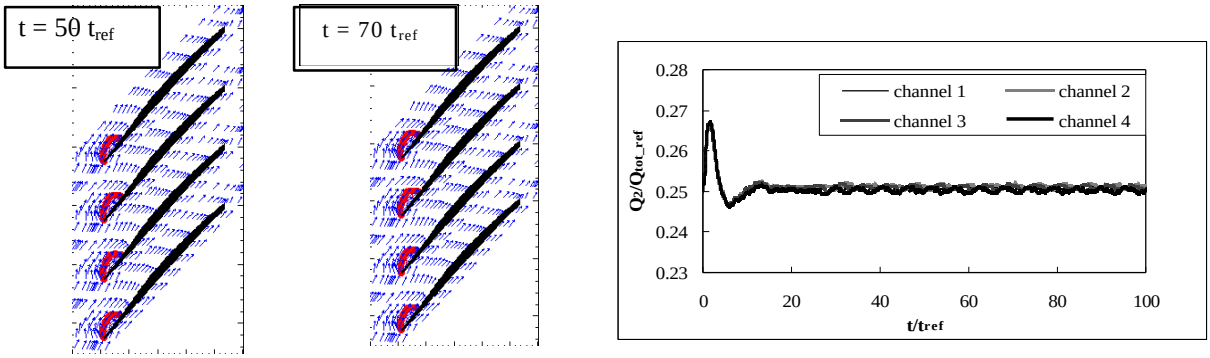

Figure 11. Multiple channels computations:
a) Cavitation behaviour at $\phi = \phi_{ref}$ and $\sigma \approx 0.1$ b) Flow rate repartition in the 4 channels.

When the cavity length is increased, an unsteady configuration spontaneously appears. Figure 12 shows that the cavities are then different on the successive blades. The unbalanced cavitating structure propagates from blade to blade in time. Figure 13 shows the repartition of the flow rate in the cascade. After the initial transient, periodic fluctuations take place with different phases in the four channels. Their amplitude increases with the decreasing cavitation number.

Visual observation (Figure 12) and a FFT analysis of cavity length fluctuations signal show that in stator frame the phenomenon is about 50% faster than the inducer rotation speed. As observed in the experiments, this value slightly decreases with cavitation parameter. However, the numerical frequencies of that super synchronous phenomenon remain about 25% larger than experimental values, as already observed in analytical models (Tsujimoto *et al*., 1993; Joussellin & de Bernardi, 1994).

For a lower cavitation parameter a stable configuration appears (Figure 14), with alternate long and short cavities on the blades and different flow rates in the successive channels. Such a configuration is observed experimentally but at a σ higher than the super synchronous range.

Figure 15 shows the cavitating performance computed by averaging the head coefficient obtained with the 4 channels simulations at fixed cavitation number and flow rate coefficient (points Δ). In the non-symmetric range, the head coefficient is then larger than the one obtained from the single-channel computation. On the other hand, the final head drop is reached at higher σ, because of the lack of symmetry.

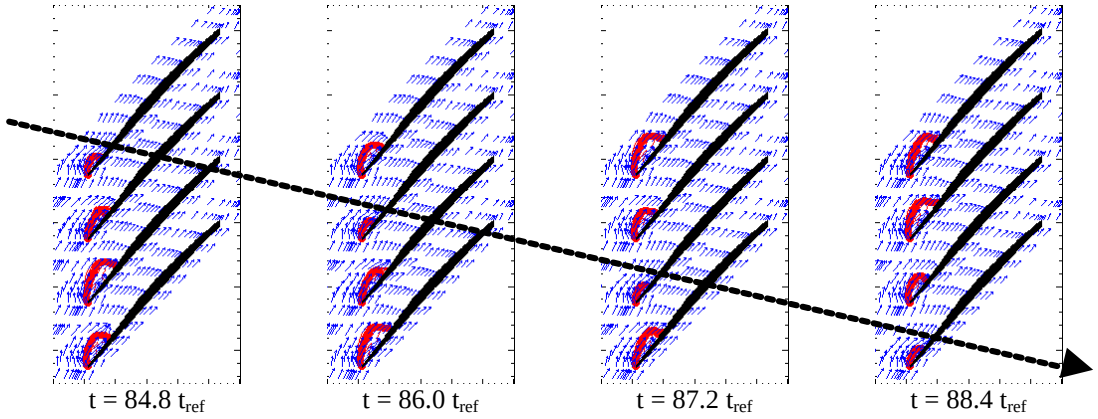

Figure 12. Cavitation behaviour at $\phi = \phi_{ref}$ and $\sigma \approx 0.097$.

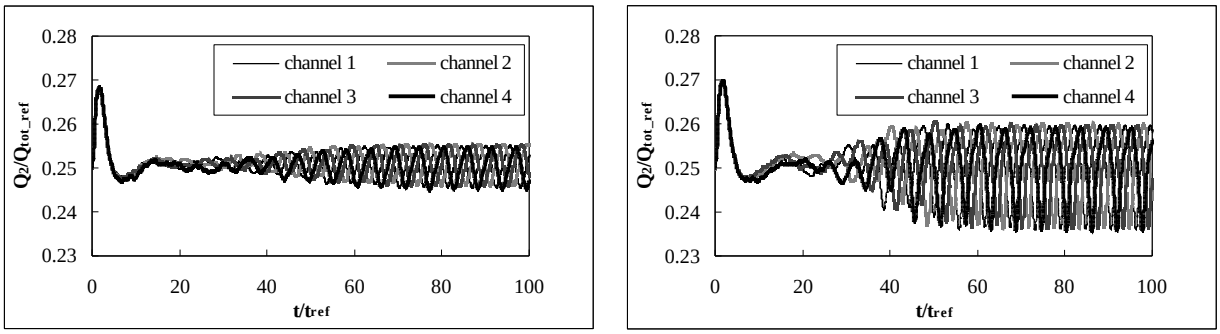

Figure 13. Flow rate repartition in the 4 channels, $\phi = \phi_{ref}$; a) $\sigma \approx 0.097$; b) $\sigma \approx 0.086$.

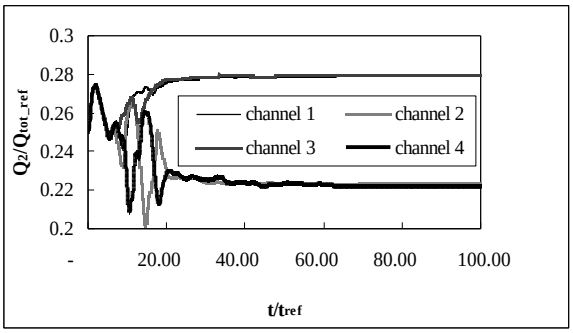

Figure 14. Flow rate repartition in the 4 channels, $\phi = \phi_{ref}$, $\sigma \approx 0.052$

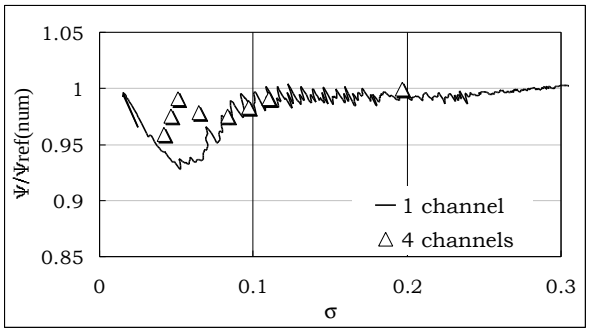

Figure 15. Cavitation characteristic of the cascade: comparison between single-channel and 4-channels computations, $\phi = \phi_{ref}$

7. Conclusion: comparison between experimental and numerical results

Computations were performed at different operating conditions. Numerical results allow to draw the cavitating performance of the blade cascade at different flow rates and to identify the limit of the rotating cavitation behaviour. In the different cases, the final head drop is predicted by the model at a σ about 0.02 too high with respect to the experimental value (0.04 instead of 0.02). The cavitation parameter range of rotating cavitation $\Delta\sigma = (\sigma_+ - \sigma_-)$;, increases when the flow rate coefficient decreases (Figure 16 and Table 1). That result agrees with experimental observations (Pagnier *et al.* 1995, Yokata *et al.*, 1999). At reference flow rate, ϕ_{ref} the experimental instability range is about $\Delta\sigma_{exp} = 0.025$ (Figure 1). Numerical results of $\Delta\sigma$ are plotted with respect to the flow rate coefficient in Table 1: the comparison shows that experimental range correspond to the numerical result at ϕ/ϕ_{ref} between 1.05 and 1.1. That result agrees qualitatively with the previous analysis that the obstruction due to the cavitating backflow modifies the cascade inlet condition. Further work is now needed to assess the prediction capability of the model. Therefore, improvements of the analysis of 3D inlet flows and study of the influence of the cascade design by

numerical simulations are in progress, in parallel to the development of a full 3D model (Coutier-Delgosha *et al*,. 2001).

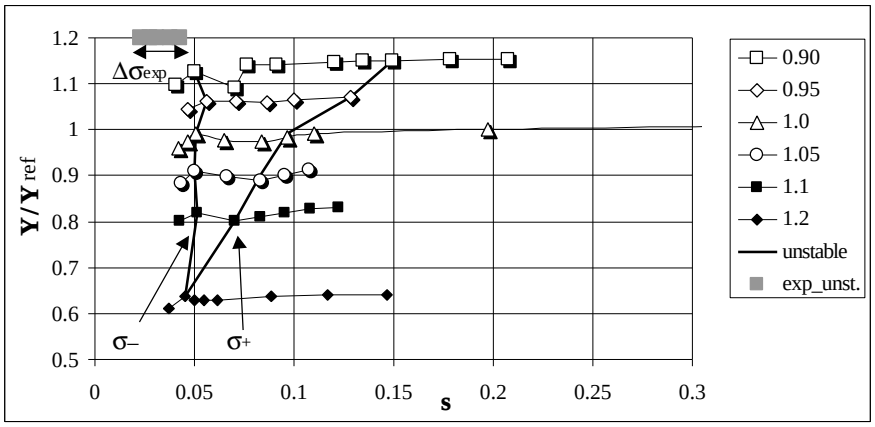

Figure 16. Effet of the flow rate on the cavitation characteristic and on the instability range (comparison with the experimental instability range in grey)

f/f_{ref}	Ds
0.90	0.099
0.95	0.072
1.0	0.046
1.05	0.033
1.1	0.018
1.2	0

Table 1: Instability range versus flow coefficient.

Acknowledgments

The authors wish to thank SNECMA Moteurs (Rocket Engine Division) and the French space agency CNES for their support to the present work. The CREMHyG laboratory - Grenoble, France - provided the experimental results.

References

COUTIER-DELGOSHA O., REBOUD J-L.& ALBANO G. (2000). Numerical Simulation of the Unsteady Cavitating Behaviour of an Inducer Blade Cascade. *Proc. ASME Fluids Engineering Summer Conference*. Boston Massachusetts.

COUTIER-DELGOSHA O., REBOUD J-L.& FORTES-PATELLA R. (2001). Numerical study of the effect of the leading edge shape on cavitation around inducer blade sections. *4th Int. Symp. on Cavitation*, Pasadena, California.

de BERNARDI J., JOUSSELLIN F.&VON KAENEL A.(1993). Experimental Analysis of Instabilities Related to Cavitation in Turbopump Inducer. *1st Int. Symp. on Pump Noise and Vibrations*, pp. 91-99. Paris, France.

DELANNOY, Y. & KUENY, J.L. (1990). Two phase flow approach in unsteady cavitation modelling. *Cavitation and Multiphase Flow Forum,* ASME-FED vol.98, pp. 153-158.

GOIRAND B., MERTZ A., JOUSSELLIN F. & REBATTET C. (1992) Experimental Investigation of Radial Loads Induced by Partial Cavitation with Liquid Hydrogen Induce. *3rd Int. Conf. on Cavitation, ImechE, C453/056*, pp. 263-269. Cambridge, U.K.

JOUSSELLIN F. & DE BERNARDI J. (1994). Analytical Modelling of Instabilities in a Cavitating Turbopump Inducer. In *2nd Int. Symp. on Cavitation*, pp. 98-94, Tokyo, Japan.

JOUSSELLIN F. , MAITRE T. & MOREL P. (1998). 3D Cavity shape in an inducer :Experimental investigations and numerical predictions. *3rd Int. Symp. on Cavitation,* Grenoble, France.

KAMIJO K., SHIMURA T. & WATANABE M. (1977) An Experimental Investigation of Cavitating Inducer Instability. *ASME Paper 77-WA/FW-14*.

LABORDE R., CHANTREL P., RETAILLEAU A., MORY M. & BOULON O. (1995). Tip Clearance Cavitation in an Axial Flow Pump. In *Cav'95 Int. Symp,*. Deauville, France.

PAGNIER P, MOREL P., SPETTEL F., HENRY C &CHAMPAGNE J-Y. (1995). Conception and experimental study of an inducer. In *Cav'95 Int. Symp.,* Deauville, France.

PETROV V. & CHEBAYEVSKY V. (1973). *Cavitation Characteristics of High-Rotational Centrifugal Pumps with Inducers*, Mashinostroyenie.

PILIPENKO V., SEMYONOV Y. & KVASHA Y. (1995). Theoretical and Experimental Computational Methods for Determining Volume of Cavities and Coefficients of Dynamic Equation of Cavitation Cavities. *Tech. Rep*.. SEP TC/T 23227/96.

REBOUD J-L. & DELANNOY Y.(1994). Two-phase flow modelling of unsteady cavitation. *2nd Int. Symp. on Cavitation,* Tokyo.

TSUJIMOTO Y. KAMIJO K. & YOSHIDA Y. (1993). A Theoretical Analysis of Rotating Cavitation Inducers. *J. Fluids Eng.* **115**, pp. 135-141.

VON KAENEL A., MAITRE T., REBATTET C., KUENY J.L.& MOREL P. (1995). Three dimensional partial cavitating flow in a rocket turbopump inducer: numerical predictions compared with laser velocimetry measurements, *Cav'95 Int. Symp.,* Deauville, France.

WATANABE, S., TSUJIMOTO, Y., FRANC, J.-P. & MICHEL, J.-M. (1998). Linear Analyses of Cavitation Instabilities. *3rd Int. Symp. on Cavitation*, pp. 347-352. Grenoble, France.

YOKATA K., KURAHARA K., KATAOKA D., TSUJIMOTO Y. & ACOSTA A.J. (1999). A Study on Swirling Backflow and Vortex Structures at the inlet of Inducer. *JSME Int. Journal, Series B,* Vol.**42-3**, 451-459.